

# Localization of Fiducial Skin Markers in MR Images using Correlation Pattern Recognition for PET/MRI Nonrigid Breast Image Registration

Derek Walvoord<sup>1</sup>, Karl G. Baum<sup>1</sup>, María Helguera<sup>1</sup>, Andrzej Krol<sup>2</sup>, Roger Easton<sup>1</sup>

<sup>1</sup> Chester F. Carlson Center for Imaging Science at the Rochester Institute of Technology, Rochester, NY, 14623 USA

<sup>2</sup> Radiology Department at SUNY Upstate Medical University, Syracuse, NY, 13210 USA

**Abstract** - In most instances, multiple-modality visualization of pathologies will present advantages over single-modality studies. For many medical imaging procedures, it is desirable to produce a “fused” output that simultaneously exhibits characteristics of the data from each individual modality to reduce the difficulty of the decision-making process for radiologists. Preprocessing for most data fusion algorithms typically performs the necessary registration of the input data (from each modality). Fiducial markers may be used to display image locations that are common to each modality if the images exhibit very different spatial structure, as is the case with MRI and PET imagery. The process of automating the detection of these markers needs more investigation in the medical field, and the current state of the art often requires manual selection by a human observer throughout the 3-dimensional image stack. The objective of automated detection is to locate the centroid of each marker in a noisy background that contains additional objects that span a large range of intensity values. The correlation methods employed must somehow “normalize” the images to accommodate changes in the input image, so that “brightness” of the region does not affect the correlation, thus reducing the false positive rate. The filter should accommodate within-class distortion, as the size and shape of the fiducial marker will vary through the image stack. For this work, a mean-subtracted MACH filter was constructed and applied to data that are mean-subtracted locally. The location of centroids in the output stack of correlation planes was determined by applying morphological operations to extract regions-of-interest. It is apparent that a relatively high probability of detection is obtained over a wide range of thresholds with an acceptable false positive rate.

## I. INTRODUCTION

In most instances, multiple-modality visualization of pathologies will present advantages over single-modality studies. The benefits stemming from acquisition of medical images from multiple instruments have begun to outweigh the additional cost. Images from different modalities, such

as X-ray computed tomography (CT), magnetic resonance imaging (MRI), single photon emission computer tomography (SPECT), positron emission tomography (PET), and ultrasound are used to acquire complementary information. For example, an MRI or CT image might be acquired to obtain the anatomical information followed by the acquisition of one or more PET or SPECT images to obtain information on the physiological and/or functional behavior in the areas of interest.

The spatial relationships between the modalities must be evaluated and conveyed to the observer to maximize the benefits from multimodal images. The process of calculating the spatial relationships between the images and manipulating the data so that corresponding pixels appear at the same physical location is called *image registration*. Algorithms for image fusion combine the registered images into a single image.

The advantage of a fused image accrues from the inability of human observers to visually judge spatial relationships between images viewed side by side. Depending on background texture, mottle, shades and colors, identical shapes and lines may appear to be different sizes [1]. The most obvious application is to combine a functional image that identifies a region of interest with an anatomical image that provides structural information.

### *Multimodal Breast Cancer Imaging*

Application of a multimodality approach is advantageous for detection, diagnosis, and management of breast cancer. In this context, F-18-FDG positron emission tomography (PET) [2,3] and high-resolution and dynamic contrast-enhanced magnetic resonance imaging (MRI) [4,5] have steadily gained the acceptance of X-ray mammography and

ultrasonography. Initial experience with combined PET (functional imaging) and X-ray computed tomography (CT, anatomical localization) exhibit significant improvements in diagnostic accuracy and enable better differentiation between normal and pathological uptake and by providing positive finding in CT images for lesions with low metabolic activity, e.g., in bowel) [3].

Coregistration of PET and MRI images provides additional information on morphology (including borders, edema, and vascularization) and on dynamic behavior (including fast wash-in, positive enhancement intensity, and fast wash-out) of the suspicious lesion and allows more accurate lesion localization, including mapping of hyper- and hypometabolic regions as well as better lesion-boundary definition. Such information might be of great value for assessing breast cancer and assessing the need for biopsy. Any subsequent biopsy could be precisely guided to the most metabolically active (i.e., the most malignant) region.

The task of registration [6-9] and fusion [9-12] of PET and MRI breast images has been addressed by the authors. However, the registration method used in those cases has limited clinical use due to the level of human interaction. Image processing techniques may be used to automate much of the process and thus reduce operator time to an acceptable level. One of the more time-consuming tasks of the registration process is determination of the location of fiducial skin markers placed on the surface of the breast prior to imaging. This paper presents a method for automatic localization of fiducial skin markers (FSMs) in magnetic resonance images.

### Registration

The breast is composed entirely of soft tissue and easily deforms, so that multimodal imaging requires nonrigid registration. Physically deformable breast models are very difficult to implement because of complex patient-specific breast morphology and highly nonlinear and difficult to measure elastic properties of different types of tissues in the breast, as well as explicitly unknown boundary conditions [6]. The approach for nonrigid coregistration of multimodal images presented here overcomes these difficulties because no information about patient-specific breast morphology and elastic tissue properties are required.

Identical positioning of patients is used to ensure similar stress conditions while obtaining images from both modalities. The registration is a two-step process. During the first step, displacement of the corresponding fiducial skin markers (FSMs) is used to calculate a displacement field over the entire breast. The specially prepared FSMs are taped to predefined locations on the skin prior to data acquisition and are visible in all modalities. A dense displacement field is estimated by first distributing the observed FSM displacement vectors linearly over the breast surface and then distributing throughout the volume. This process has been implemented using standard finite-element

method (FEM) software. Using the resulting displacement field, the MRI image, can be warped to the PET image (Fig. 1).

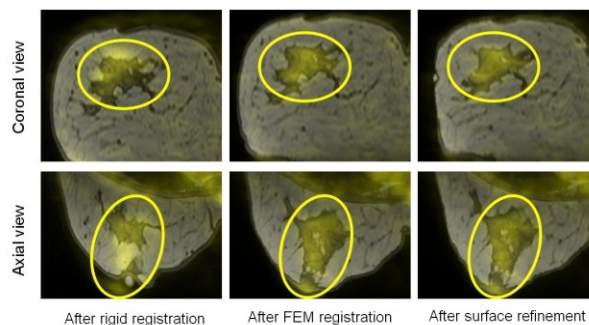


Fig. 1. Registered and fused PET and MRI breast images. Yellow: PET. Gray: MRI. The suspicious lesion area is circled.

Since small registration errors still exist in regions away from the FSMs, a surface refinement process is performed. During this phase of registration a large number of corresponding surface points are identified on the warped MRI image and the CT image of the breast that is obtained just before PET (using a PET/CT scanner), and that is coregistered with the PET image. The displacement vectors found between the corresponding points in the MRI and CT images are then used to deform the mesh a second time. A displacement field provided by the mesh is then used to create the registered image (Fig. 1). More information about this registration process can be found in [6-9].

## II. FILTER DESIGN

The process of automating the detection of FSMs in medicine has not been widely investigated. Current methods often require manual selection by a human observer throughout the 3-dimensional image stack. To further demonstrate the flexibility of the correlated pattern recognition (CPR) system, the design was improved to accommodate full MRI image stacks such that the centroid locations of markers could be determined using the correlation techniques in the filter library. This task takes full advantage of the inherent shift invariance of spatial correlation, which permits detection over the entire scene.

The fiducial skin markers in the MRI data exhibit a nearly spherical ellipsoidal shape and relatively high contrast. When progressing through the image stack, the size of an individual marker increases to its maximum cross-sectional area and then decreases until the stack no longer intersects the 3-dimensional marker. Thus, the volume of a marker is represented by image slices containing the approximate area, which also increases to a maximum and then decreases.

The objective is to detect and locate the centroid of each marker within a noisy background that contains additional objects with a large range of intensity values. Thus, the markers can not be segmented by simple thresholds or adaptive thresholds. Any correlation methods must evaluate

some “normalizing” characteristic, similar to that provided by the correlation coefficient.

The normalized correlation coefficient accommodates variations in the intensity in the input image, so that objects that do not share similar spatial structure with the reference pattern are assigned small values in the output correlation plane, effectively reducing the false alarm rate. We also need to evaluate the capability of the filter to accommodate within-class distortion due to the variation in size and shape of the fiducial marker through the image stack. Thus, we seek a composite correlation design that has been “corrected” for normalization.

Of the possible filters that may be used, the Maximum Average Correlation Height (MACH) filter [14,15] exhibits tolerance to both distortion and noise. It is a composite filter aimed at minimizing the average similarity measure (ASM) between output correlation planes from each training image used to construct the filter mask. In addition, the MACH filter simultaneously maximizes the average correlation height (ACH) of the output. The lexicographically ordered transfer function  $\mathbf{h}$  for the MACH filter is shown in Eq. (1):

$$\underline{h} = \gamma \mathbf{C} + \mathbf{I} \underline{m} \quad (1)$$

where

$$\underline{S} = \frac{1}{N \times d} \sum_{i=1}^B X_i - M \mathbf{C}_i - M \quad (2)$$

The transfer function  $\mathbf{h}$  is lexicographically ordered as a column vector,  $\mathbf{I}$  is the identity matrix (which minimizes the effects of white noise),  $\mathbf{x}$  is the column vector of the average training image,  $\mathbf{m}$  is the column vector consisting of the average Fourier transforms from the training images, and  $\mathbf{X}$  and  $\mathbf{M}$  are diagonal matrices containing the elements in  $\mathbf{x}$  and  $\mathbf{m}$ .  $N$ ,  $d$ , and  $\sigma$  are scalar constants: the number of training images, the number of pixels and a normalization constant, respectively.

The MACH filter is a composite filter that is very similar to the simple crosscorrelation with the mean training image. If  $\mathbf{C} = \mathbf{I}$  (as is this case), then Eq. 1 becomes the crosscorrelation for a training set consisting of a single training image. The numerator of the expression cancels the phase due to translation and filters out components with large spatial frequencies that contain noise and sharp edges (assuming the training image is dominated by low-frequency components). At frequencies that exhibit a large deviation between the individual exemplars and the mean, the magnitude of the filter output is reduced. The same is true for frequencies with a large contribution from noise. Conversely, if the sum of the noise and the deviation within the training set is smaller than unity at a particular frequency, the MACH filter will amplify the corresponding frequency in the output. Thus, the MACH filter can be interpreted as the mean-training crosscorrelation with weights applied to each frequency to control attenuation and amplification based on the ASM and noise.

### Implementation

For this work, a mean-subtracted MACH filter was constructed and applied to input stacks that were mean-subtracted locally over  $32 \times 32$  pixel regions, which is the size of the training. Fig. 2 shows the training exemplars used to produce the desired transfer function.

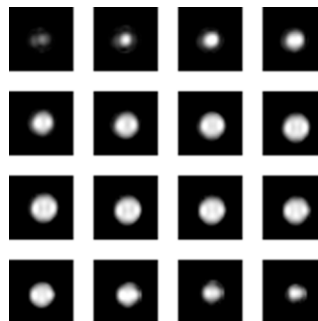


Fig. 2. Training exemplars extracted from a single fiducial skin marker

The output image stack of correlation planes was analyzed to determine the centroids of each marker by first selecting and applying a global threshold (i.e., over the entire image stack). Once the binary stack is produced, the 4-neighbor connected components specify each region by a nonzero value. The mean  $x$ ,  $y$ , and  $z$  coordinate of each region are calculated and used as the possible locations of the centroids.

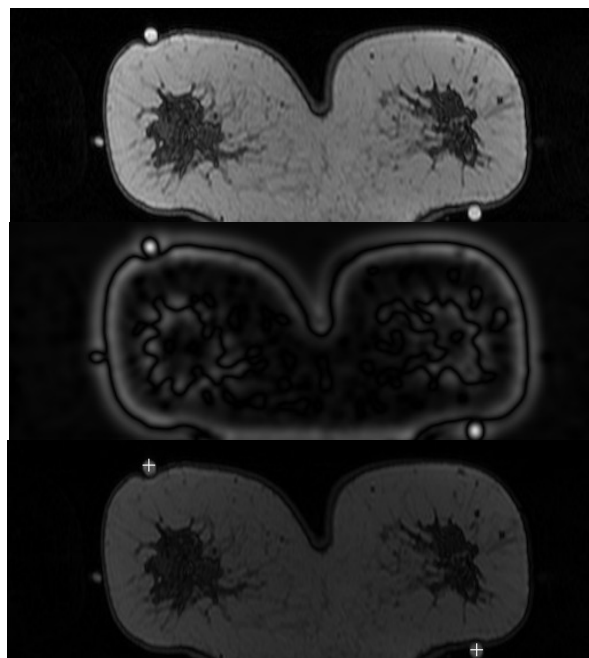


Fig.3. Slice 110 from the 3-dimensional MRI image stack (Top) before preprocessing to subtract the local mean, (Middle) after correlation with a mean-subtracted MACH filter, and (Bottom) post-processed to show the centroid locations of registration markers. Note that the leftmost marker was detected, but its centroid lies further through the image stack.

To reduce the number of false alarms, a region-growing algorithm is implemented at each potential centroid. If the volume of the resulting region lies between predefined thresholds determined from the geometry of the fiducial markers, the algorithm assumes that the centroid location corresponds to one of the fiducial skin markers. Fig. 3 shows a slice from a 3-dimensional MRI image stack after each of the three stages of this algorithm.

### III. RESULTS AND CONCLUSIONS

Preliminary results were obtained using the training set in Fig. 2 and MRI image stacks from five individuals. Each image included between nine and eighteen fiducial markers. Adjustment of the level of the global threshold applied to the correlation output either increases or decreases the number of regions computed via connected components. Obviously, if the global threshold is set too high, some peaks in the correlation output that correspond to locations of markers may be lost. Conversely, if the threshold is set too low, many regions in the correlation output must be analyzed as potential locations for markers, effectively increasing the discrimination task and false alarm rate.

Fig. 4 shows the ROC curve produced for this data set after applying the algorithm discussed in this section. The plot in Fig. 5 is included to show the global thresholds that were used as the operating points of the ROC curve.

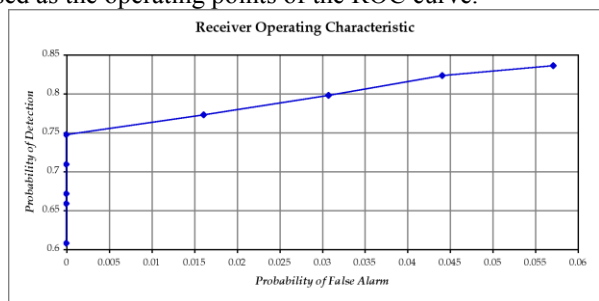


Fig. 4. The ROC curve produced after applying CPR to classify fiducial skin markers from 3-dimensional MRI image stacks of five individuals.

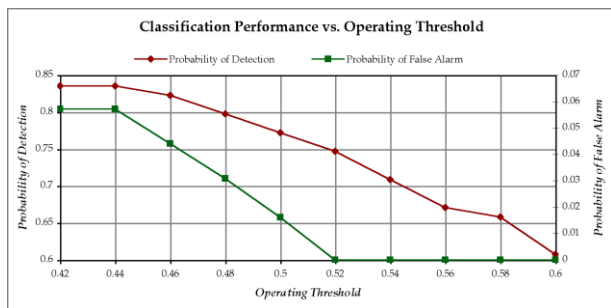


Fig. 5. The global thresholds applied to the correlation output to control the operating point on the ROC curve.

An operating threshold of 0.5 corresponds to a threshold of 50% of the global maximum applied to the full correlated output image stack. It is apparent that a relatively high probability of detection is obtained for a wide range of

thresholds for an acceptable false alarm rate. A noticeable problem is that the algorithm does not detect all markers even after drastically lowering the global threshold. This obstacle is due to the poor contrast characteristic of slices at the beginning and end of the image stacks. Methods of preprocessing the MRI data prior to implementation of the correlation algorithm are being considered for future work.

### ACKNOWLEDGMENT

The authors would like to acknowledge the efforts of J. A. Mandel, I. L. Coman, E. D. Lipson, W. Lee, M. Z. Unlu, and A. Magri in the development of the registration procedure. They would also like to acknowledge E. Schmidt and K. Rafferty for their efforts in image fusion.

### REFERENCES

- [1] Rehm, K., S. C. Strother, J. R. Anderson, K. A. Schaper, and D. A. Rottenberg, "Display of merged multimodality brain images using interleaved pixels with independent color scales," *J Nucl Med* **35**, pp. 1815-21, 1994.
- [2] Bombardieri, E. and F. Crippa, "PET imaging in breast cancer," *Quat J Nuc Med*, **45**, pp. 245-256, 2001.
- [3] Scheidhauer, K., C. Walter, M. D. Seemann, "FDG PET and other imaging modalities in the primary diagnosis of suspicious breast lesions," *Eur J Nucl Med Mol Imaging*, **31**, Suppl. 1, S70-S79, 2004.
- [4] Eliat, P. A., and V. Dedieu, "Magnetic resonance imaging contrast-enhanced relaxometry of breast tumors: an MRI multicenter investigation concerning 100 patients," *Mag. Res. Imaging*, **22**, pp. 475-81, 2004.
- [5] Gibbs, P. and G. P. Liney, "Differentiation of benign and malignant sub-1 cm breast lesions using dynamic contrast enhanced MRI," *Breast* **13**, pp. 115-21, 2004.
- [6] Krol, A., Unlu, M. Z., Baum, K. G., Mandel, J. A., Lee, W., Coman, I. L., Lipson, E. D., Feiglin, D. H., "MRI/PET Nonrigid Breast-Image Registration Using Skin Fiducial Markers," *Physica Medica European Journal of Medical Physics*, **XXI**, Supplement 1, pp. 31-35, 2006.
- [7] Krol, A., Unlu, M. Z., Magri, A., Lipson, E., Coman, I. L., Mandel, J. A., Baum, K. G., Feiglin, D. H., "Iterative Finite Element Deformable Model For Nonrigid Coregistration of Multimodal Breast Images," *Biomedical Imaging: Macro to Nano*, IEEE International Symposium, pp. 852-855, 2006.
- [8] Krol, A., Coman, I. L., Mandel, J. A., Baum, K. G., Luo, M., Feiglin, D. H., Lipson, E. D., Beaumont, J., "Inter-Modality Non-Rigid Breast Image Registration Using Finite-Element Method," *Nuclear Science Symposium Conference Record*, IEEE, **3**, pp. 1958-1961, 2003.
- [9] Baum, K. G., "Multimodal Breast Imaging: Registration, Visualization, and Image Synthesis," PhD Dissertation, Rochester Institute of Technology, Chester F. Carlson Center for Imaging Science, 2008.
- [10] Rafferty, K., Baum, K. G., Schmidt, E., Krol, A., Helguera, M., "Multimodal Display Techniques with Application to Breast Imaging," RIT Digital Media Library, 2007.
- [11] Baum, K. G., Helguera, M., Krol, A., "Fusion Viewer: A New Tool for Fusion and Visualization of Multimodal Medical Data Sets," *Journal of Digital Imaging*, in press.
- [12] Baum, K. G., Helguera, M., Krol, A., "Genetic Algorithm Automated Generation of Multivariate Color Tables for Visualization of Multimodal Medical Data Sets," *Proc. 14<sup>th</sup> Color Imaging Conference*, IS&T/SID, pp. 138-143, 2006.
- [13] A. Samani, J. Bishop, D. B. Plewes, "A Constrained Modulus Reconstruction Technique for Breast Cancer Assessment," *IEEE Trans. Med. Imaging* **20**(9), 877-885, 2001.
- [14] B. V. K. Vijaya Kumar, A. Mahalanobis, and R. D. Juday, *Correlation Pattern Recognition*, Cambridge University Press, New York, 2005.
- [15] B. V. K. Vijaya Kumar and A. Mahalanobis, "Recent advances in composite correlation filter designs," *Asian Journal of Physics*, **8**(3), 1999.